Nanoscale

COMMUNICATION

View Article Online
View Journal | View Issue

Cite this: *Nanoscale*, 2015, **7**, 1661

Received 28th October 2014,
Accepted 21st November 2014

DOI: 10.1039/c4nr06340f

www.rsc.org/nanoscale

A magnetic polyaniline nanohybrid for MR imaging and redox sensing of cancer cells†

Yoochan Hong,‡[a,b] Seungyeon Hwang,‡[b,c] Dan Heo,[b,c] Bongjune Kim,[d] Minhee Ku,[b,e] Eugene Lee,[b,c] Seungjoo Haam,[d,f] Dae Sung Yoon,[g] Jaemoon Yang*[b,f] and Jin-Suck Suh*[b,f]

A synthetic process for constructing an organo-metal nanohybrid is described. This process uses polyaniline as a ligand in order to fabricate magnetic nanoparticles. This nanohybrid shows imaging potential uses as a magnetic resonance imaging contrast agent and a redox-sensing probe simultaneously both *in vitro* and *in vivo*.

Recently, multifunctional nanostructures have been designed by researchers.[1–4] In particular, magnetic nanoparticles (MNPs) composed of iron have been used for magnetic resonance (MR) imaging as drug delivery carriers.[5] The MR imaging potential of MNPs occurs from their remagnetization response to a magnetic field.[6] On the other hand, one of the most reported conducting polymers, polyaniline (PAni), has attracted significant interest due to its easy synthesis and high conductivity, the reversibility of its oxidation/reduction processes, the facile controllability of its redox state by doping, and the varying colors of its different redox states.[7,8] PAni is especially interesting as a material for biosensors, because it can act as an effective mediator for electron transfer in redox and enzymatic reactions.[9] The role of PAni as a mediator is due to the presence of delocalized redox charges over a series of conducting grains (polarons) in its crystallite emeraldine salt-I phase.[10] PAni is considered to be an attractive polymer since it exhibits two redox couples in the appropriate range to facilitate an enzyme–polymer charge transfer and thereby acts as a self-contained electron transfer mediator.

Herein, we suggest the use of bifunctionally magnetic PAni nanohybrids (MPNHs) for MR imaging and redox sensing of the cancer cell microenvironment. MPNHs consist of MNPs that function as MR contrast agents, and PAni acts as a redox-sensing agent. The sensing of the redox state in biological systems occurs because the redox state is related to the regulation of protein activity, cell signaling, gene transcription, and various cellular events in response to reactive oxygen species.[11–14] To synthesize water-soluble nanoprobes, MPNHs are functionalized with maleimidyl-TWEEN 80 (MPNHm), and MPNHm shows potential as an MR contrast agent by solution MR imaging. Moreover, the synthesized MPNHm shows the reversibility of its color changes with changing pH conditions as also an original characteristic of PAni. Subsequently, MPNHm was conjugated with a peptide (MPNHm–P), which can be targeted toward one of the representative biomarkers of invasive cancer cells, membrane type 1-matrix metalloproteinase (MT1-MMP). MPNHm–P confirmed the redox-sensing potential and targeting ability in an MT1-MMP-overexpressing cell line (HT1080) compared to a low-expressing cell line (MCF7). Furthermore, MPNHm–P was injected into the tumor site of a xenograft mouse model directly. *In vivo* MR and optical images were used to show the potential of the MR contrast agent and the redox-sensing agent, respectively (Scheme 1).

To verify the fabrication of MPNHs in the steady state, transmission electron microscopy (TEM) imaging was preferentially conducted. Fig. 1a–d show TEM images of MPNHs synthesized by various molar ratios of iron(III) acetylacetonate(I), and PAni (P). The synthetic process for MPNHs is derived from the thermal decomposition method, one of the methods for the synthesis of magnetic nanoparticles. Briefly, iron(III) acetylacetonate and PAni acted as a precursor and a ligand, respectively. Other synthetic parameters were adjusted to the previous thermal decomposition method, such as solvents, temperature, and reaction time. A detailed synthetic method is described in the ESI.† In Fig. 1a, without using PAni (I : P = 10 : 0), single

[a]*Department of Biomedical Engineering, Yonsei University, Maeji 234, Heungup, Wonju, Gangwondo, Republic of Korea 220-710*
[b]*Department of Radiology, College of Medicine, Yonsei University, Shinchon, Seodaemoon, Seoul, Republic of Korea 120-752. E-mail: 177hum@yuhs.ac, jss@yuhs.ac*
[c]*Nanomedical National Core Research Center, Yonsei University, Shinchon, Seodaemoon, Seoul, Republic of Korea 120-749*
[d]*Department of Chemical and Biomolecular Engineering, Yonsei University, Shinchon, Seodaemoon, Seoul, Republic of Korea 120-749*
[e]*Brain Korea 21 Plus Project for Medical Science, Yonsei University, Shinchon, Seodaemoon, Seoul, Republic of Korea 120-752*
[f]*YUHS-KRIBB Medical Convergence Research Institute, Shinchon, Seodaemoon, Seoul, Republic of Korea 120-752*
[g]*School of Biomedical Engineering, Korea University, Anam 5, Seingbuk, Seoul, Republic of Korea 136-701*
†Electronic supplementary information (ESI) available. See DOI: 10.1039/c4nr06340f
‡These authors contributed equally to this work.

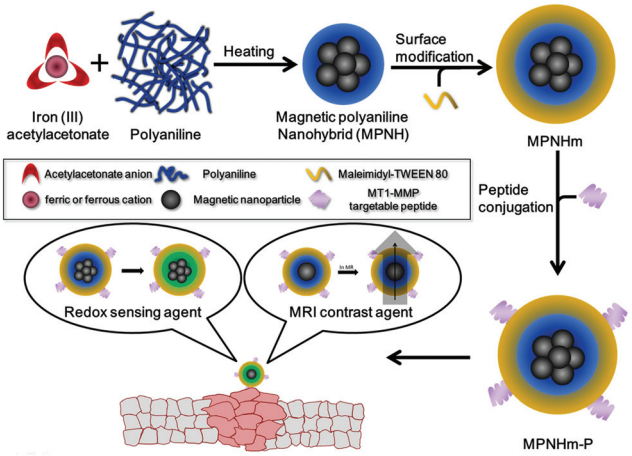

Scheme 1 Schematic illustration of the synthesis of a magnetic polyaniline nanohybrid (MPNH) as an MR imaging and redox-sensing agent.

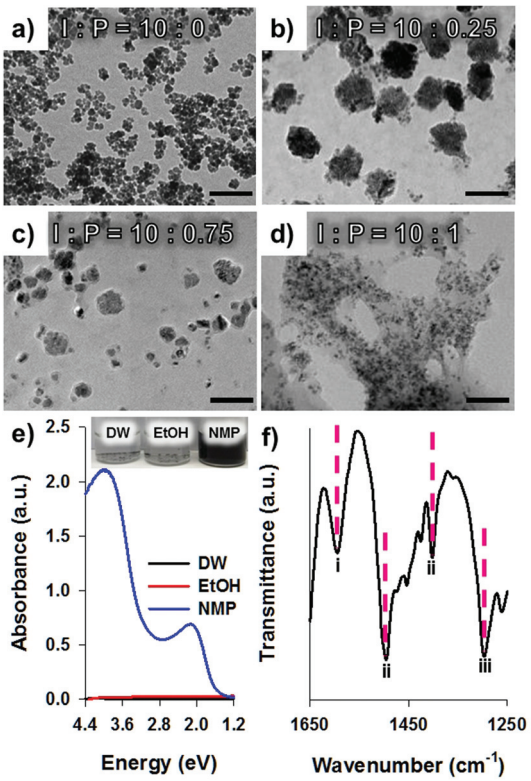

Fig. 1 TEM images of MPNH in the following ratios for iron(I) and PAni (P): (a) 10 : 0, (b) 10 : 0.25, (c) 10 : 0.75, and (d) 10 : 1. All sale bars are 100 nm. (e) Absorbance spectra for MPNHs dispersed in the indicated solvents. Inset is a photograph for solutions containing PAni in the indicated solvents. (f) FTIR spectra for MPNHs. The Roman characters (i, ii, and iii) represent interesting peaks described in more detail in the text.

MNPs of 10.3 ± 4.3 nm were irregularly clustered and showed no PAni coating. In Fig. 1b, an increased molar ratio of PAni (I : P = 10 : 0.25) induced the regular self-assembly of single MNPs with PAni coating and showed a narrow size distribution of MPNHs of 71.3 ± 5.6 nm. In Fig. 1c, it can be seen that the clustering tendency between single MNPs decreased, and MPNHs lost their spherical shapes due to the increased PAni molar ratio (I : P = 10 : 0.75). In Fig. 1d (I : P = 10 : 1), the spherical shape of the particles was not found by TEM, and MPNHs formed a large area of the PAni cloud containing MNPs. From these results, we decided that the conditions in Fig. 1b were ideal for the synthesis of MPNHs, and the following experiments were conducted using this approach. The presence of PAni in MPNHs was shown using a solubility test for MPNHs, with deionized water (DW), ethanol (EtOH), and *N*-methyl-2-pyrrolidone (NMP). As described in Fig. 1e, with either DW or EtOH, MPNHs had poor solubility and aggregated and precipitated. In contrast to this result, with NMP, MPNHs were well dispersed and had a higher solubility than either DW or EtOH. These effects seem to be caused by one of the representative characteristics of PAni, which involves MNP. As described in a previously published report,[8] PAni has better solubility in NMP than in DW, and we also observe this solubility property in MPNHs. The absorbance spectra also show the presence of PAni as well as the solubility of MPNHs toward DW, EtOH, and NMP. Because of the aggregation and precipitation of MPNHs in DW and EtOH, the absorbance spectra of MPNHs in those cases cannot be measured, but in NMP, the correct absorbance spectrum can be obtained. These results are proof of the involvement of PAni with MNP, and are consistent with a previously published report.[4] The chemical structure of MPNHs was confirmed by peaks in the Fourier transform infrared (FTIR) spectra: 1580 cm^{-1} (C=C and N=Q=N stretching of the quinoid ring, denoted as (i), 1400 and 1495 cm^{-1} (C=N stretching of the quinoid ring, denoted as (ii), and 1300 cm^{-1} (aromatic C–N stretching of benzenoid rings, denoted as (iii) (Fig. 1f). The results in Fig. 1 show that MPNHs can be successfully fabricated in a nanohybrid form, and PAni is well contained in the MPNH as we expected.

In order to increase the capability of MPNHs as MR contrast agents and redox-sensing agents in biological systems, a nanoprecipitation method was applied to improve the solubility and stability of MPNHs in water.[8] Maleimidyl-TWEEN 80 was used as a surfactant; as a result, the surface of the MPNH was modified with a maleimidyl group (MPNHm). To investigate the influence of the doping property by PAni, the MPNHm was doped using various pH solutions (pH 1–10). Fig. 2a shows the effect of pH on the optical properties of the MPNHm. At low pH (pH < 2), MPNHm was converted into the ES (green color) state. At higher pH (pH > 3), MPNHm transitioned to an EB state (blue color). The absorbance spectra of MPNHm over a range of pH values were measured (Fig. 2b). At pH 1, PAni nanoparticles were in the doped state (ES), as indicated by the presence of the π–π* transition of the benzenoid rings as well as the polaron band transitions at about 2.95 and 1.30–1.55 eV. With decreasing HCl concentrations, the polaron bands at 2.95 and 1.30–1.55 eV gradually decreased in intensity, and a strong absorbance band at about 2.14 eV was observed. The absorbance band at 2.14 eV is attributed to excitation from the highest occupied molecular orbital of the three-ring benzenoid structure of PAni to the lowest unoccupied molecular orbital of

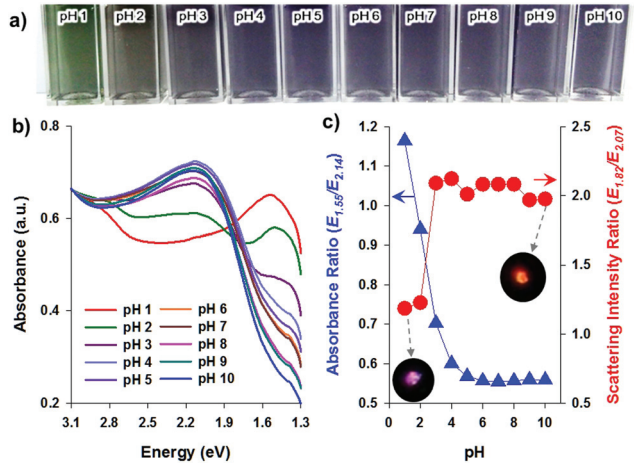

Fig. 2 (a) A photograph of MPNHm in the indicated pH solutions. (b) Absorbance spectra for MPNHm in pH 1–10. (c) Absorbance ratio ($E_{1.55}/E_{2.14}$, triangle) and scattering intensity ratio ($E_{1.82}/E_{2.07}$, circle) for MPNHm as a function of pH. Insets represent light scattering images of MPNHm in the state of ES (pH 1) and EB (pH 10), respectively.

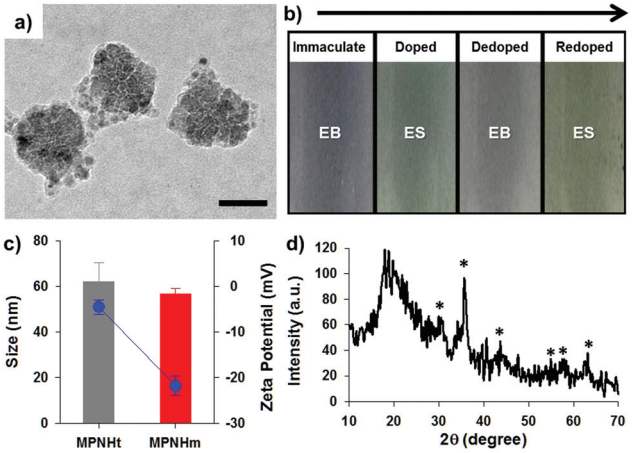

Fig. 3 (a) A TEM image of MPNHm after the conjugation of maleimidyl-TWEEN 80. (b) A photograph of MPNHm solutions changing state. (c) Size and zeta potential for MPNHt and MPNHm. (d) XRD pattern of MPNHm. The peaks of the Fe_3O_4 nanocrystal structure are marked with asterisks (*).

the localized quinoid ring and the two surrounding imine nitrogens in the EB state of the PAni nanoparticles. In order to distinguish more quantitatively between the EB and ES states of MPNHm, the absorbance ratios ($E_{1.55}/E_{2.14}$) were calculated at the representative energies of the peaks for the EB ($E_{1.55}$) and ES ($E_{2.14}$) states (Fig. 2c). As the pH value increased from 1 to 6, the absorbance ratio decreased also, but it did not change further at the higher pH value (pH > 7). Additionally, to confirm the capability of redox sensing of MPNHm in biological systems, scattering spectra of a single MPNHm molecule were measured, and darkfield imaging of MPNHm was also conducted by varying the pH. As shown in Fig. 2c, scattering intensity ratios dramatically transited between pH 2 and pH 3. Visualizing darkfield microscopic images of MPNHm, the EB state of MPNHm appeared as a bright orange color, and the ES state of MPNHm appeared as a dark red color. These darkfield imaging results are consistent with the results of the absorbance spectra. Generally, objects can be said to have the color of light leaving their surfaces, that is, the human eye can perceive the color of objects by receiving the reflected energy of light from the object. The absorbance spectra demonstrate that the energy of the valley is related to the reflected energy; in MPNHm, the valley energy of the EB state (pH 3–10) corresponds to 2.91 eV. This energy value represents a blue color, and for pH values 1 and 2, the valley energies match the color of each solution, respectively. In the darkfield microscopic images, on the other hand, the reflected light does not reach the eyepiece, but only the scattered light reaches our eye; therefore, we can show the complementary color of the object in the darkfield microscopic images. As shown in the insets of Fig. 2c, on the darkfield microscopic images, the color of MPNHm in the ES state (pH 1) is shown as a dark red color, which corresponds to the complementary color of green, and the color of MPNHm in the EB state (pH 10) is shown as a bright orange color, which corresponds to the complementary color of blue, respectively. Collectively, these results indicate that MPNHm can be doped with H^+ ions and their counterions, and also suggests that the spectral changes and darkfield images of MPNHm can be used to determine the specific redox state of a biological system.

For the *in vitro* and *in vivo* MR imaging and redox sensing of cancer, hydrophobic MPNH was coated by MPNHm and dispersed in water (Fig. 3a). To study the redox-sensing ability, the MPNHm solution underwent repetitive doping and dedoping processes, and showed reversible green (ES) and blue (EB) changes (Fig. 3b). For the confirmation of successful coating of maleimidyl-TWEEN 80 on the surface of MPNH, the hydrodynamic diameter was measured *via* the dynamic light scattering method. MPNH was also coated with plain TWEEN 80 (MPNHt) as a control nanoparticle toward MPNHm. The hydrodynamic diameter showed no significant changes (MPNHt: 62.2 ± 9.7 nm, MPNHm: 57.4 ± 2.3 nm) (Fig. 3c). X-ray diffraction (XRD) was used to obtain the structural information of Fe_3O_4 in MPNHm (Fig. 3d). The XRD patterns of MPNHm showed that the MNPs contained in MPNHm were of a highly crystalline inverse spinel structure. The position diffraction peaks matched well with those of the magnetite powder. The magnetic hysteresis curves of MPNHm in the EB and ES states support the potential of MPNHm as an MR contrast agent (Fig. 3d).

To confirm the magnetic property of MPNHm, a vibrating sample magnetometer (VSM) was used. MPNHm in the EB state showed a superparamagnetic property with saturation magnetization at 3.8 emu g^{-1}. However, in the ES state, MPNHm shows a diamagnetic property, because MNPs contained in MPNHm dissolved and only PAni remained. As described in previously published reports, it is a well-known phenomenon that iron oxide dissolves in acidic environments,[15,16] and this phenomenon was also confirmed in the case of the MPNHm *via* VSM in Fig. 4a. To confirm the poten-

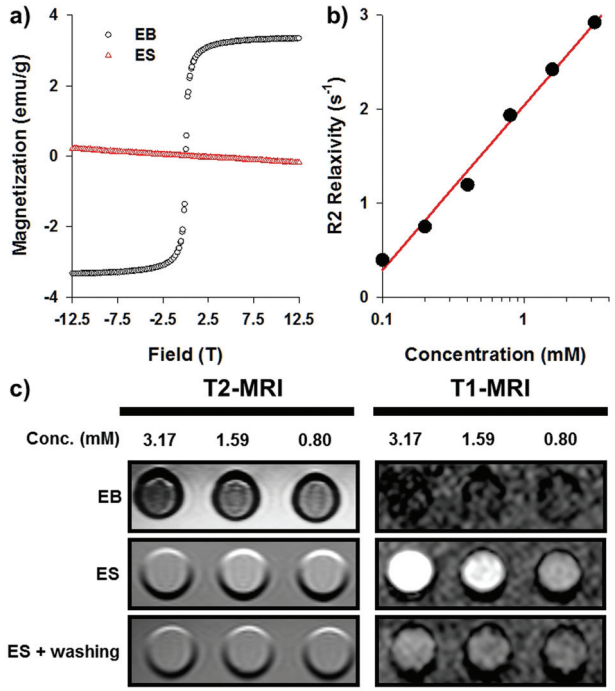

Fig. 4 (a) Magnetic hysteresis loops for MPNHm in EB (black circle) and ES (red triangle) states. (b) R_2 relaxivity of MPNHm in the EB state. (c) T_2- and T_1-MR images for MPNHm in EB, ES, and ES states after washing at the indicated concentrations.

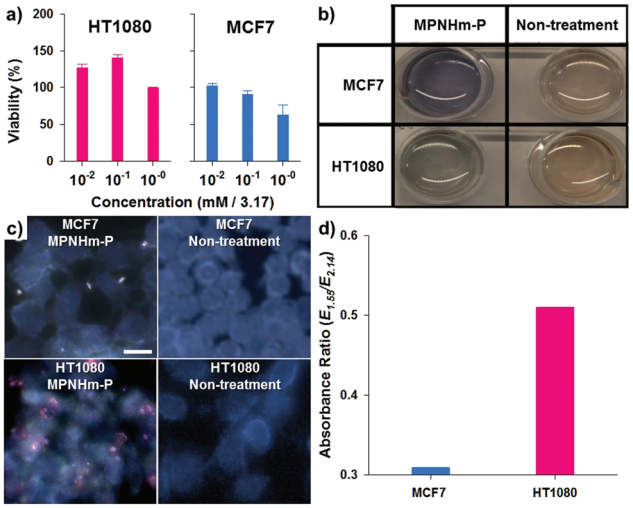

Fig. 5 (a) Cell viability test of MPNHm–P in HT1080 and MCF7 cells. (b) Photographs of MCF7 and HT1080 cells with or without MPNHm–P. (c) Darkfield microscopic images of MCF7 (first row) and HT1080 (second row) cells with (the first column) or without (the second column) MPNHm–P. Scale bar is 10 μm. (d) Absorbance ratios ($E_{1.55}$/$E_{2.14}$) for MCF7 and HT1080 cells treated with MPNHm–P.

tial of MPNHm as an MR imaging contrast agent, R_2 relaxivity values are plotted as a function of the Fe concentration of MPNHm (Fig. 4b), as the R_2 relaxivity of MPNHm linearly increased according to the increase of Fe concentration in MPNHm. Furthermore, solution MR imaging of MPNHm under EB and ES states after washing was also performed (Fig. 4c). In the EB state, MPNHm successfully showed an increasing darkening contrast effect on T_2 MR imaging with increasing iron concentrations, but no changes were seen on T_1 MR imaging. In the ES state, MNPs contained in MPNHm were dissolved in acid; the iron ions showed no T_2 contrast enhancing effect but showed significant brightening on T_1 MR imaging. After washing in the ES state, MPNHm had no MNPs or iron ions, and showed no contrast enhancement effects on either T_2 or T_1 MR imaging. From the results of Fig. 3 and 4, we confirmed that MPNHm contained both PAni and iron oxide, and MPNHm shows potential as a redox-sensing agent *via* reversible doping experiments, as well as potential as a MR imaging contrast agent *via* VSM and solution MR imaging results.

To prepare the cancer MR imaging and redox-sensing probes based on MPNHm, an MT1-MMP-specific peptide was selected as a targeting moiety. MT1-MMP is a kind of specific metalloproteinase and plays a key role in cancer metastasis.[17,18] An MT1-MMP-targeting peptide was designed to include a cysteine, which contains a thiol functional group and can be conjugated simply with the maleimidyl group of MPNHm at a suitable pH.[19] MT1-MMP-targeting peptide-conjugated MPNH (MPNHm–P) was synthesized by simply mixing the MT1-MMP-targeting peptide and MPNHm. To evaluate the biocompatibility of MPNHm–P, a cytotoxicity analysis was conducted (Fig. 5a). HT1080 and MCF7 cells were selected as the highly expressing MT1-MMP group and control group, respectively, because of their different MT1-MMP expression levels.[20] The cytotoxicities of MPNHm–P in HT1080 and MCF7 cells were evaluated using the MTT assay for three different concentrations; the highest concentration, 3.17 mM, was diluted 10-fold twice. Neither HT1080 nor the MCF7 cells were damaged significantly by the treatment with the range of MPNHm–P concentrations used in this study. In Fig. 5b, images were obtained after a 24 h treatment of HT1080 and MCF7 cells with EB state-MPNHm–P. MPNHm–P was observed as the ES state color (green) in HT1080 cells, but in MCF7 cells, the EB state (blue) of MPNHm–P was maintained. This result demonstrates that MPNHm–P has cell-redox-state sensing and MT1-MMP targeting abilities. To precisely examine the ability of MPNHm–P as a colorimetric probe on a microscopic scale, darkfield microscopy was carried out (Fig. 5c). In HT1080 cells, MPNHm–P bound to the surfaces of HT1080 cells and appeared in an ES state as in Fig. 2c. In MCF7 cells, however, few or no MPNHm–P was observed, because MCF7 cells have a relatively lower expression level of MT1-MMP than HT1080 cells. The ES state of PAni allows PAni to receive biological dopants from biological systems, and these biological dopants (*i.e.* H^+ ions) are a representative material participating in redox reactions. In addition to this finding, PAni is also known as a nanoprobe that can sense various biological dopants, including one of the products of cancer metabolism, such as lactic acid or oxidative species, as well as H^+ ions.[7,8] In HT1080 cells, these biological dopants

from cancer cells may participate in changes in PAni from the EB to the ES state. The absorbance ratio ($E_{1.55}/E_{2.14}$) of HT1080 cells was also observed to be higher than in MCF7 cells, that is, MPNHm–P is in a ES-like state in HT1080 cells (Fig. 5d). These results show that MPNH is suitable for the sensing of the redox state of cancer cells using changes in its color *via* various methods (naked eye, spectrophotometer, and darkfield microscopic analysis). Collectively, the results from Fig. 3–5 show that MPNHs are suitable as *in vitro* MR contrast agents and *in vitro* redox-sensing agents, because MPNHs have properties of both MNPs (MR contrast agent) and PAni (redox-sensing agent).

To investigate the *in vivo* MT1-MMP-targeting ability of MPNHm–P using MR or optical imaging, we prepared xenograft mice models *via* the implantation of HT1080 cells at the proximal thigh. MR imaging of MT1-MMP-expressing fibrosarcomas was obtained after the injection of MPNHm–P into the tail vein of the mice (200 μg iron) (Fig. 6a and b). Before the injection of the solution (pre-injection), each T_2-weighted MR imaging of the tumor site appeared characteristically bright, with a low R_2 value. Following the injection of MPNHm–P, we observed that the tumor sites showed darkened images caused by the presence of magnetic components. These results demonstrate that MPNHm–P was effectively targeted and bound to MT1-MMP in the tumor tissue. To quantify these results, MR imaging was evaluated quantitatively by a R_2 relaxivity calculation (Fig. 6c). The R_2 value increased in comparison with the pre-injection state. *In vivo* near infrared (NIR) imaging studies were also performed to evaluate the possibility of using MPNHm–P as a redox-sensing probe to detect HT1080 cells based on MT1-MMP expression (data not shown), and the total photon counts of NIR absorbance images in the tumor site were estimated (Fig. 6d). The total photon counts indicate the number of photons received from the reflected light of examined materials at the photon detector, and lower photon counts in absorbance images suggest that photons reaching the detector are also low; in other words, lower photon counts also indicate that the absorbance of the measured object is high in the absorbance image. As described in Fig. 5d, after the MPNHm–P injection, the total photon counts were lower than those at pre-injection. This phenomenon indicates that reflected photons from the tumor site post-injection are lower than pre-injection, that is, the tumor site after MPNHm–P injection has a higher absorbance than pre-injection. To determine the precise regions detected by MPNHm–P, histological analysis was performed on the harvested HT1080 tumor tissues after MPNHm–P treatment and MR imaging. The dark purple region in the H&E-stained tissues clearly outlines the tumor (Fig. 6e), as the tumor tissue has dense, large cancer cells, with much nuclear material. The selective accumulation of MPNHm–P within the cells was verified using Prussian blue staining (Fig. 6f). Iron ions from MPNHm–P bound to the HT1080 tumors combined with the ferrocyanide result in the formation of a bright blue pigment called Prussian blue. These results demonstrate that HT1080 cells, which express high levels of MT1-MMP, were successfully targeted by MPNHm–P *in vivo*.

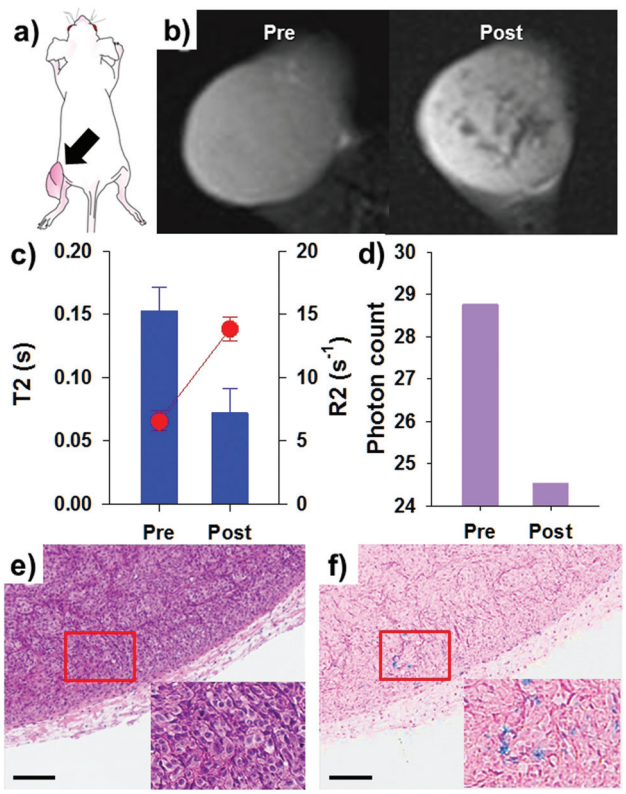

Fig. 6 (a) A HT1080 xenograft mouse. The arrow points to the tumor site. (b) *In vivo* T_2-weighted MR images both pre-injection and 120 minutes after injection of MPNHm–P. (c) T_2 relaxation time (bar) and R_2 for images in (a). (d) Photon counts corresponding to tumor specificity of MPNHm–P. (e) H&E and (f) Prussian blue staining images for tumor tissue sections. Scale bars are 100 μm. Insets are magnified images of the rectangular regions.

Conclusions

In conclusion, we designed a multifunctional nanohybrid that could act as an MR imaging contrast agent and a redox-sensing agent; this nanohybrid was successfully used for dual modal imaging. The nanohybrid has a magnetic property as well as the characteristics of PAni, and we verified that the nanohybrid could be used as an MR contrast agent and redox-sensing agent both *in vitro* and *in vivo*. We suggest that this nanohybrid could potentially lead to diagnoses of cancer by various methods, such as MR imaging or redox sensing.

Acknowledgements

This work was supported by the National Research Foundation of Korea (NRF) funded by the Ministry of Education, Science and Technology (2010-0023202 and 2012R1A2A1A01011328) and a grant from the National R&D Program for Cancer Control, Ministry for Health and Welfare, Republic of Korea (1220100).

Notes and references

1 J. Yang, C.-H. Lee, H.-J. Ko, J.-S. Suh, H.-G. Yoon, K. Lee, Y.-M. Huh and S. Haam, *Angew. Chem., Int. Ed.*, 2007, **46**, 8836–8839.
2 J. Lee, J. Yang, H. Ko, S. Oh, J. Kang, J. Son, K. Lee, S. W. Lee, H. G. Yoon, J. S. Suh, Y. M. Huh and S. Haam, *Adv. Funct. Mater.*, 2008, **18**, 258–264.
3 H. Park, J. Yang, S. Seo, K. Kim, J. Suh, D. Kim, S. Haam and K.-H. Yoo, *Small*, 2008, **4**, 192–196.
4 H. Park, J. Yang, J. Lee, S. Haam, I.-H. Choi and K.-H. Yoo, *ACS Nano*, 2009, **3**, 2919–2926.
5 J. Yang, C.-H. Lee, H.-J. Ko, J.-S. Suh, H.-G. Yoon, K. Lee, Y.-M. Huh and S. Haam, *Angew. Chem., Int. Ed.*, 2007, **46**, 8836.
6 P. W. Goodwill, E. U. Saritas, L. R. Croft, T. N. Kim, K. M. Krishnan, D. V. Schaffer and S. M. Conolly, *Adv. Mater.*, 2012, **24**, 3870.
7 J. Yang, J. Choi, D. Bang, E. Kim, E.-K. Lim, H. Park, J.-S. Suh, K. Lee, K.-H. Yoo, E.-K. Kim, Y.-M. Huh and S. Haam, *Angew. Chem., Int. Ed.*, 2011, **50**, 441.
8 J. Choi, Y. Hong, E. Lee, M.-H. Kim, D. S. Yoon, J.-S. Suh, Y.-M. Huh, S. Haam and J. Yang, *Nano Res.*, 2013, **6**, 356.
9 L. Shi, Y. Xiao and I. Willner, *Electrochem. Commun.*, 2004, **6**, 1057.
10 A. Wolter, P. Rannou, J. P. Travers, B. Gilles and D. Djurado, *Phys. Rev. B: Condens. Matter*, 1998, **58**, 7637.
11 S. Ueda, H. Nakamura, H. Masutani, T. Sasada, S. Yonehara, A. Takabayashi, Y. Yamaoka and J. Yodoi, *J. Immunol.*, 1998, **161**, 6689.
12 C. C. Winterbourn and M. B. Hampton, *Free Radicals Biol. Med.*, 2008, **45**, 549.
13 D. A. I. Mavridou, E. Saridakis, P. Kritsiligkou, A. D. Goddard, J. M. Stevens, S. J. Ferguson and C. Redfield, *J. Biol. Chem.*, 2011, **286**, 24943.
14 Y. Wang, J. Yang and J. Yi, *Antioxid. Redox Signaling*, 2012, **16**, 649.
15 D. Panias, M. Taxiarchou, I. Douni, I. Paspaliaris and A. Kontopoulos, *Can. Metall. Q.*, 1996, **35**, 363–373.
16 S. O. Lee, T. Tran, B. H. Jung, S. J. Kim and M. J. Kim, *Hydrometallurgy*, 2007, **87**, 91.
17 M. Kajita, Y. Itoh, T. Chiba, H. Mori, A. Okada, H. Kinoh and M. Seiki, *J. Cell Biol.*, 2001, **153**, 893.
18 K. Wolf, I. Mazo, H. Leung, K. Engelke, U. H. von Andrian, E. I. Deryugina, A. Y. Strongin, E.-B. Bröcker and P. Friedl, *J. Cell Biol.*, 2003, **160**, 267.
19 S. S. Ghosh, P. M. Kao, A. W. McCue and H. L. Chappelle, *Bioconjugate Chem.*, 1990, **1**, 71–76.
20 D. V. Rozanov, E. I. Deryugina, B. I. Ratnikov, E. Z. Monosov, G. N. Marchenko, J. P. Quigley and A. Y. Strongin, *J. Biol. Chem.*, 2001, **276**, 25705.